Journal of Communications Technology and Electronics, Vol. 47, No. 7, 2002, pp. 739–747. Translated from Radiotekhnika i Elektronika, Vol. 47, No. 7, 2002, pp. 822–830.

ELECTRODYNAMICS AND WAVE PROPAGATION

Determination of the Characteristics of Ionospheric Perturbations in the Near-Field Region of an Earthquake Epicenter

E. L. Afraimovich, V. V. Kiryushkin, and N. P. Perevalova

Received August 17, 2001

Abstract—Two methods are proposed for determining the spatial–temporal characteristics of ionospheric perturbations (IPs) recorded in the near-field region of a source. Using space–time processing of the distribution of total electron content (TEC) variations in the spherical wavefront approximation, the IP source coordinates and velocity are determined at the height where the *F*-region of the ionosphere is characterized by the maximum electron density. The IP source coordinates and the IP phase velocity averaged over all the altitudes where the ionosphere substantially contributes to the TEC forming are found from simulations of TEC measurements involved in the GPS ionosphere sounding. The efficiency of these methods is estimated by analyzing the distribution of TEC variations observed during the June 4, 2000, South Sumatra earthquake.

INTRODUCTION

Recently, considerable attention has been given to the study of ionospheric responses to shock acoustic waves (SAWs) [1] generated by rocket launches, industrial explosions, and earthquakes. Such ionospheric perturbations were recorded using various methods of remote ionosphere diagnosis: vertical and oblique HF sounding [1–3], the method involving measurements of the Faraday rotation of the signal polarization plane during transionospheric sounding by UHF radio signals from geostationary artificial Earth satellites (AESs) [4–6], and GPS ionosphere sounding [7–11]. At present, the basic parameters of ionospheric responses to SAWs (the waveform, amplitude, and period) are well studied. Determination of the spatial–temporal characteristics of these ionospheric perturbations is now more topical and involves a wide variety of problems, such as measurements of the IP phase and group velocities, determination of the IP propagation direction and the perturbation source location, and the analysis of the SAW waveform and propagation dynamics, which is a more general problem. The remote diagnosis of the ionosphere using transionospheric sounding by two-frequency GPS navigation signals is most suitable for solving these problems.

A method using three spaced GPS receivers is developed for determining the IP phase velocity and propagation direction, as well as the coordinates of an IP source [12, 13]. Another method is developed for determining the phase velocity and the IP arrival direction [14]. It is based on space–time processing of the distribution of the ionospheric TEC variations reconstructed from GPS measurements. However, these methods can be applied only in the case when the IP wavefront slightly differs from the flat one within the TEC distribution region under study. Therefore, determination of the characteristics of ionospheric perturbations recorded in the near-field region of a point source, where the spherical wavefront cannot be approximated by a plane, remains to be a topical problem.

In this paper, the following two methods for solving this problem are presented: the method of space–time processing of the TEC variation distribution in the spherical-wavefront approximation (in what follows, the space–time processing method) and the method using simulations of the TEC measurements involved in GPS ionosphere sounding (in what follows, the simulation method). Both methods allow determination of the IP phase velocity and source location. The efficiency of the proposed methods is estimated by analyzing the distribution of the TEC variations caused by SAWs induced by the June 4, 2000, South Sumatra earthquake (the magnitude was 7.7, the coordinates of the epicenter were $\Phi_e = -4.72°$ and $\Lambda_e = 102.1°$, and the time of the underground shock was $t_0 = 16:28:26$ (16.475) UT). In this case, we use the simplified model where the epicenter source of earthquake-induced SAWs is replaced by the surface point source located at the earthquake epicenter [15] and the SAW front is a semisphere propagating above the Earth's surface.

1. TESTING OF THE IONOSPHERIC RESPONSES FOR THEIR LOCATION IN THE NEAR-FIELD REGION OF THE EARTHQUAKE EPICENTER

The initial data for forming the space–time distribution of the ionospheric responses to SAWs are the temporal series of HF TEC variations $\Delta I(t)$ and the corresponding series of the azimuthal ($\alpha_{sat}(t)$) and elevation $\theta_{sat}(t)$) angles of the line-of-sight (LOS) oriented towards a satellite. The raw TEC temporal series $\Delta I(t)$ are filtered by removing the linear trend (the 5-min time

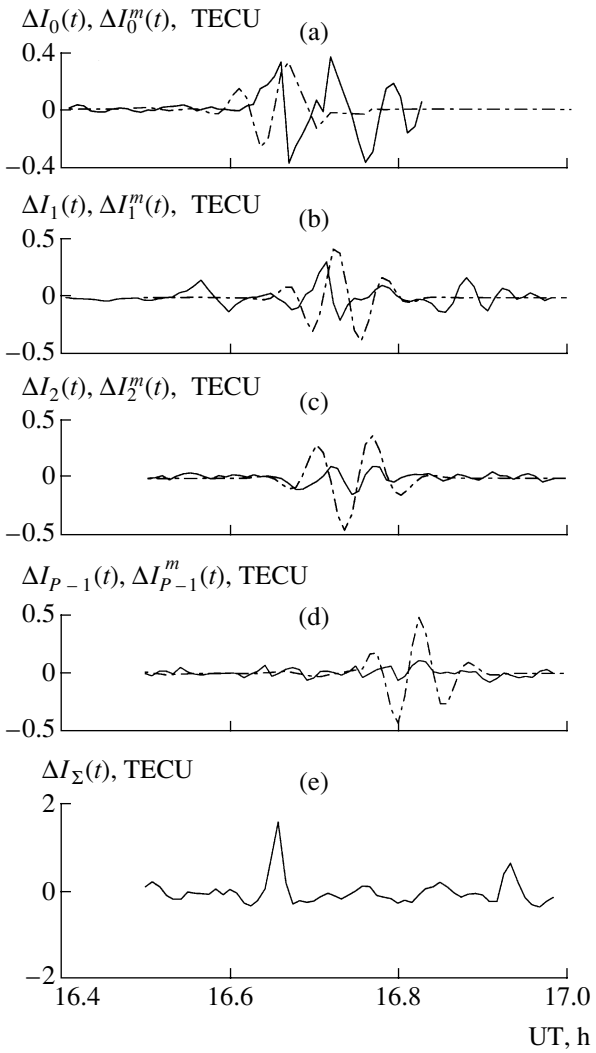

Fig. 1. (solid line) Experimental $\Delta I_i(t)$ and (dashed line) synthetic $\Delta I_i^m(t)$ TEC variation temporal series for the SIPs of the following LOSs: (a) NTUS—15, (b) NTUS—21, (c) SAMP—03, …, (d) SAMP—15. (e) Total spatial assembly signal $\Delta I_\Sigma(t)$.

window is used). The TEC values are reconstructed from the phase delays of GPS two-frequency navigation signals propagating along the GPS receiver–satellite LOS. The corresponding TEC reconstruction procedure described in detail in [8, 11–13] is not discussed in this paper. The 5-min length of the time window used for removing the trend is determined by the period of the SAW IP caused by rocket launches, earthquakes, and industrial explosions. This period does not exceed 300 s [3–13].

Series $\Delta I(t)$ and the corresponding series of $\theta_{sat}(t)$ and $\alpha_{sat}(t)$ are calculated using the CONVTEC software developed at the Institute of Solar–Terrestrial Physics (Siberian Division of Russian Academy of Sciences) and converting RINEX files (standard for the GPS system) downloaded from the Internet.

At the time of the June 4, 2000, South Sumatra earthquake, the measurements were conducted with the use of nine LOSs from GPS receivers NTUS, BAKO, and SAMP to GPS satellites nos. PRN03, PRN15, and PRN21.[1] The parameters of recorded ionospheric responses to SAWs are as follows: amplitude A ranges from 0.1 to 0.5 TECU and the perturbation period ranges from 151 to 331 s (see Table 1).[2] These results are in good agreement with the data obtained by other authors [2, 8, 11–13], which indicates the stable ionospheric signal signatures of the earthquake IP.

The plots of $\Delta I_i(t)$ (solid line) for the four GPS receiver–satellite LOSs (NTUS—15, NTUS—21, SAMP—03, and SAMP—15) are presented in Figs. 1a–1d. It is seen from the figures that, for these LOSs, the variations $\Delta I_i(t)$ are well correlated and shifted relative to each other along the time axis. It is assumed that an ionospheric response is recorded at moment t_{max} when the TEC perturbation amplitude reaches its maximum.

To eliminate the uncertainty in the localization of the ionospheric response to the SAWs due to the integral nature of TEC, we suppose that the TEC is formed at the subionospheric point (SIP) which is the point of intersection of the LOS oriented towards a satellite with the plane at altitude h_{max} where the F region of the ionosphere is characterized by the maximum ionization mainly contributing to the TEC formation. The geographical coordinates of the SIP (Φ and Λ) are defined as the coordinates of its projection on the Earth's surface. The name of the SIP obtained corresponds to the GPS receiver–satellite LOS. On calculating the SIP coordinates for moment t_{max}, we determine the location of the ionospheric response to the SAW in space. In this case, the LOS directed to the satellite depends on $\theta_{sat}(t)$ and $\alpha_{sat}(t)$ obtained at t_{max}.

Having determined $t_{max,\,i}$ for each series $\Delta I_i(t)$ and the corresponding SIP coordinates (Φ_i and Λ_i), we find the space–time distribution of ionospheric responses to SAWs (Fig. 2). For each GPS receiver–satellite LOS used for recording ionospheric responses, the values of $t_{max,\,i}$, Φ_i, and Λ_i are summarized in Table 1.

For convenience of further calculations, the SIP latitude and longitude are converted to Cartesian horizontal coordinates (x_i, y_i) of the topocentric coordinate system whose origin coincides with a certain SIP (reference point O (x_0, y_0)). The location of the ionospheric response with the minimum value of t_{max} is regarded as a reference point. For the event under consideration, it is the NTUS–15 LOS SIP corresponding to $t_{max,\,0}$ =

[1] PRN (Pseudo Random Noise) is the notation of a satellite number conventional in the GPS.

[2] TECU (Total Electron Content Units) is the unit TEC equal to 10^{16} m^{-2}.

16.658 UT. Then, for the NTUS GPS station and the PRN15 GPS satellite, TEC temporal series $\Delta I_0(t)$ with the removed trend can also be regarded as a reference one.

Since the methods proposed can be applied only in the near-field region of a perturbation source, it is necessary to estimate locations of recorded ionospheric responses to SAWs relative to the IP source far-field region boundary in order to find out whether it is possible to use these methods for analyzing the distribution obtained. For equiphase condition interval $\Delta\varphi = \pi/4$, the relationship between the radius of the IP source far-field region R_{fr} and linear dimension L of the zone where the ionospheric responses to SAWs are distributed has the form

$$R_{\text{fr}} = 4L^2/\lambda, \quad (1)$$

where λ is the IP wavelength. If the signals recorded at different SIPs are in-phase within the above equiphase condition interval and the wavefront is plane, the phase shift $\Delta\varphi = \pi/4$ of these signals corresponds to the time interval $T/8$. For the average value of the SAW-induced IP period T = 200 s [3–13], this time interval is 25 s, which is within the error of the GPS measurements performed at the 30-s data sampling interval.

For the South Sumatra earthquake, the IP source far-field region boundary is determined by the radius R_{fr} = 16000 km with allowance for the average values of L (L = 900 km) and λ (λ = 200 km). Horizontal distance $\rho_{h,i}$ of ionospheric responses from the earthquake epicenter ranges between 230 and 700 km, i.e., $\rho_{h,i} < R_{\text{fr}}$, and the epicenter is inside the region where the SIPs are distributed (see Fig. 2). Consequently, the ionospheric responses to SAWs are recorded in the near-field region of the earthquake epicenter, which allows using the proposed methods for determining the IP characteristics.

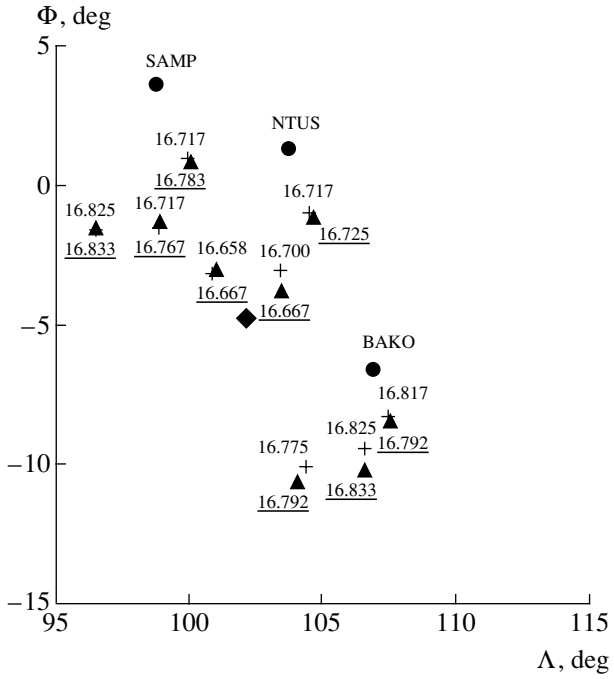

Fig. 2. Location map of the experiment. The black circles indicate the locations of the GPS stations, the crosses show the locations of the experimental SIPs at the time of the maximum ionospheric response (the time $t_{\max,i}$ is indicated next to these crosses); the triangles denote the locations of the SIPs at the time of the synthetic response maximum, the underlined numbers are moments $t^m_{\max,i}$. The black rhomb shows the earthquake epicenter.

2. SPACE–TIME PROCESSING

The space–time processing algorithm discussed in detail in [14] is reduced to the summation of series

Table 1. Basic parameters of the ionospheric responses to SAWs at the time of the earthquake

GPS receiver–satellite LOS	GPS measurements					Simulation		
	$t_{\max,i}$, h UT	Φ_i, deg	Λ_i, deg	A_i, TECU	T_i, s	$t^m_{\max,i}$, h UT	Φ^m_i, deg	Λ^m_i, deg
SAMP–03	16.717	–1.50	98.83	0.097	208	16.767	–1.32	98.92
NTUS–03	16.700	–3.03	103.41	0.473	331	16.667	–3.82	103.43
BAKO–03	16.825	–9.45	106.59	0.498	298	16.833	–10.28	106.56
SAMP–15	16.825	–1.57	96.52	0.108	180	16.833	–1.60	96.53
NTUS–15	16.658	–3.13	100.89	0.322	270	16.667	–3.14	101.07
BAKO–15	16.775	–10.06	104.36	0.112	208	16.792	–10.69	104.07
SAMP–21	16.717	0.96	99.95	0.235	180	16.783	0.76	100.01
NTUS–21	16.717	–0.99	104.51	0.306	237	16.725	–1.21	104.65
BAKO–21	16.817	–8.31	107.47	0.112	151	16.792	–8.55	107.54

$\Delta I_i(t)$ preliminary phased and reference series $\Delta I_0(t)$. As a result, we obtain total signal $\Delta I_\Sigma(t)$ of the spatially assembled TEC series with the removed trend (see Fig. 1e):

$$\Delta I_\Sigma(t) = \Delta I_0(t) + \sum_{i=1}^{P-1} \Delta I_i(t) \exp\left[\frac{-j2\pi\Delta\tau_i}{T}\right], \quad (2)$$

where $\exp\left[\frac{-j2\pi\Delta\tau_i}{T}\right]$ is the phasing weighting factor, T is the SAW period, $\Delta\tau_i = (t_{\max,i} - t_{\max,0})$ is the shift time of ith series $\Delta I_i(t)$ relative to reference series $\Delta I_0(t)$, and P is the number of series to be summed. Since the useful TEC oscillations due to the SAW propagation are well correlated in each of the summed series and the background noise oscillations are not correlated (see Figs. 1a–1d), the signal-to-noise ratio in the total spatial assembly signal increases by a factor of at least $\sqrt{P}$. Figure 1e illustrates this effect for the earthquake under consideration. The shift time of the summed series is

$$\Delta\tau_i = \Delta\rho_{h,i}/V_{h,i}, \quad (3)$$

where $\Delta\rho_{h,i} = \rho_{h,i} - \rho_{h,0}$ is the difference between the horizontal distances of the ith and reference SIPs from the IP source and $V_{h,i} = V/\cos\theta$ is the horizontal component of the IP phase velocity. Velocity $V_{h,i}$ depends on elevation angle θ of the wave vector of phase velocity V at the ith SIP. Assuming that the SAW front is spherical, this angle is determined by the ratio between the horizontal and radial distances of the ith SIP from the IP source

$$\cos\theta = \frac{\rho_{h,i}}{\sqrt{\rho_{h,i}^2 + h_{\max}^2}}. \quad (4)$$

The expression for $\rho_{h,i}$ is as follows:

$$\rho_{h,i} = \sqrt{(x_i - x_s)^2 + (y_i - y_s)^2}, \quad (5)$$

where (x_i, y_i) are the coordinates of the ith SIP and (x_s, y_s) are the coordinates of the IP source. In this case, we take into account that the origin of the chosen topocentric system coincides with the reference SIP (i.e., $x_0 = 0$ and $y_0 = 0$) and modify expression (3) to the form

$$\Delta\tau_i = \frac{(\sqrt{(x_i - x_s)^2 + (y_i - y_s)^2} - \sqrt{x_s^2 + y_s^2})\sqrt{(x_i - x_s)^2 + (y_i - y_s)^2}}{V\sqrt{(x_i - x_s)^2 + (y_i - y_s)^2 + h_{\max}^2}}. \quad (6)$$

Then, for the set of SIPs at which the ionospheric responses to SAWs are recorded, we have the system of $(P-1)$ equations

$$\Delta\tau_1 = \frac{(\sqrt{(x_1 - x_s)^2 + (y_1 - y_s)^2} - \sqrt{x_s^2 + y_s^2})\sqrt{(x_1 - x_s)^2 + (y_1 - y_s)^2}}{V\sqrt{(x_1 - x_s)^2 + (y_1 - y_s)^2 + h_{\max}^2}},$$

$$\Delta\tau_2 = \frac{(\sqrt{(x_2 - x_s)^2 + (y_2 - y_s)^2} - \sqrt{x_s^2 + y_s^2})\sqrt{(x_2 - x_s)^2 + (y_2 - y_s)^2}}{V\sqrt{(x_2 - x_s)^2 + (y_2 - y_s)^2 + h_{\max}^2}}, \quad (7)$$

$$\ldots\ldots\ldots\ldots\ldots\ldots\ldots\ldots\ldots\ldots\ldots\ldots\ldots\ldots\ldots\ldots\ldots\ldots\ldots\ldots,$$

$$\Delta\tau_{P-1} = \frac{(\sqrt{(x_{P-1} - x_s)^2 + (y_{P-1} - y_s)^2} - \sqrt{x_s^2 + y_s^2})\sqrt{(x_{P-1} - x_s)^2 + (y_{P-1} - y_s)^2}}{V\sqrt{(x_{P-1} - x_s)^2 + (y_{P-1} - y_s)^2 + h_{\max}^2}}.$$

The approximate solution of this system is sought numerically from the minimum condition for rms discrepancy ϵ of the right- and left-hand sides of these equations. For the South Sumatra earthquake, the minimum value $\epsilon = 0.027$ h was achieved at the phase velocity $V = 1050$ m/s and the IP source coordinates $\Phi_s = -4.0°$, and $\Lambda_s = 102.0°$. The obtained values of V, Φ_s, Λ_s, and ϵ are presented in Table 2.

Table 2. IP spatial–temporal characteristics

Method	V, m/s	Φ_u, deg	Λ_u, deg	ϵ, h
Space–time processing	900	−4.0	102.0	0.027
Simulation	700	−4.8	102.1	0.032

3. SIMULATION

The simulation method assumes that the desired spatial–temporal IP characteristics (the phase velocity and the source coordinates) are included in the set of input parameters of the TEC measurement model for the GPS ionosphere sounding. These characteristics are

chosen so that model TEC variations $\Delta I_i^m(t)$ perfectly simulate the TEC increment temporal series $\Delta I_i(t)$ obtained experimentally from the GPS measurements. Synthetic temporal series $\Delta I_i^m(t)$ are obtained in the same manner as series $\Delta I_i(t)$, namely, by eliminating the linear trend (with the 5-min time window) from TEC series $I_i^m(t)$ obtained as a result of simulation. The TEC measurement model for GPS ionosphere sounding is based on the model borrowed from [16] and includes the TEC measurement and ionization models.

In the spherical topocentric coordinate system whose origin coincides with the GPS receiver location, the simulated TEC time dependence is determined by the expressions

$$I^m(t) = \int_0^{D(t)} N(t, r, \alpha_{sat}, \theta_{sat})dr,$$
$$D(t) = \sqrt{R_{sat}^2 - R_E^2\cos^2[\theta_{sat}(t)]} - R_E\sin[\theta_{sat}(t)], \quad (8)$$

where $D(t)$ is the oblique distance along the GPS receiver–satellite LOS, R_E is the Earth's radius, $R_{sat} = R_E + h_{sat}$ is the satellite orbit radius, $N(t, r, \alpha_{sat}, \theta_{sat})$ is the local electron concentration, and r is the radius vector of a point on the GPS receiver–satellite LOS.

The actual values of $\alpha_{sat}(t)$ and $\theta_{sat}(t)$ from the RINEX files obtained by the receiving ground-based GPS stations that were located in the earthquake region were used for simulation. The altitude of the GPS satellite orbit was assumed to be $h_{sat} = 20000$ km.

It is appropriate to specify model electron concentration $N(t, R, \Phi, \Lambda)$ in the geocentric coordinate system, where x', y', and z' are the rectangular geocentric coordinates, and R (radius vector), Φ (latitude), and Λ (longitude) are the spherical geocentric coordinates.

Therefore, in order to determine local electron concentration $N(t, r, \alpha_{sat}, \theta_{sat})$ in (8), it is necessary to convert spherical topocentric coordinates (r, α_{sat}, and θ_{sat}) of a given point to spherical geocentric coordinates (R, Φ, and Λ) according to the known formulas and substitute them into the expression for $N(t, R, \Phi, \Lambda)$.

This model takes into account both the slow daily variations of N and the nonregular variations of a smaller amplitude and space scale. The ionization distribution is

$$N(t, R, \Phi, \Lambda) = N_0(R)N_t(t, \Phi, \Lambda)[1 + N_d(t, R)], \quad (9)$$

where $N_0(R)$ is the daily average spherically symmetrical distribution of N, $N_t(t, \Phi, \Lambda)$ is the function describing daily regular-ionization variations, and $N_d(t, R)$ is the nonregular structure of the electron concentration.

The radial part (altitude dependence of ionization) of the regular ionization is

$$N_0(R) = N_{max}\exp\left[-\left(\frac{R - R_E - h_{max}}{h_d}\right)^2\right], \quad (10)$$

where N_{max}, h_{max}, and h_d are the average daily parameters of the maximum ionization region: the electron concentration, height, and half-thickness, respectively. Parameter N_{max} is calculated using the experimental average daily values of critical frequency f_{0F2}.

The daily variations of $N_t(t, \Phi, \Lambda)$,

$$N_t(t, \Phi, \Lambda) = 1 + A_t\cos(\xi), \quad (11)$$

are determined by zenith angle ξ of the Sun; here, A_t is the amplitude of the daily variations relative to the mean level. Zenith angle ξ of the Sun is calculated using the number of the day and the local meridian time [17].

We assume that, at the time of the earthquake, the nonregular structure of the ionosphere is due to the spherical SAW propagating from the source. Then, we can suppose that the SAW IP is also a sphere whose "wall thickness" depends on the SAW packet (train) duration.

In order to localize the IP spherical wave, we specify, in the model, the following parameters of the source: its latitude Φ_s, longitude Λ_s, altitude h_s above the Earth's surface, and switch-on time t_s. Taking into account that the SAW propagation in the atmosphere is dispersive, the electron concentration perturbation is determined as the discrete superposition of the traveling spherical waves

$$N_d(t, R) = \sum_{j=1}^{N_w} W_{dj}(t, R)A_j\cos[\Omega_j(t - t_s) - K_j(R - R_s) + \varphi_j], \quad (12)$$

where R is the radius vector of the current point, $R_s = R_E + h_s$ is the radius vector of the perturbation source, A_j is the amplitude, Ω_j is the frequency, φ_j is the initial phase, K_j is the wave number of the jth spherical perturbation wave, N_w is the number of waves, and $W_{dj}(t, R)$ is the modulating envelope forming the wave-packet perturbation. The frequency of the spherical wave is defined as $\Omega_j = 2\pi/T_j$, where T_j is the period of the jth spherical wave. The wave phase at an arbitrary point of space is determined only by the radius vector

$$(R - R_s) = \sqrt{(x' - x_s')^2 + (y' - y_s')^2 + (z' - z_s')^2}, \quad (13)$$

from this point to the perturbation source, where (x', y', z') are the coordinates of the current point and (x_s', y_s', z_s')

are the coordinates of the perturbation source. The wave number of the *j*th spherical wave is defined as

$$K_j = 2\pi/\lambda_j, \quad (14)$$

where $\lambda_j = T_j V_j$ is the wavelength of the *j*th spherical IP wave and V_j is its phase velocity.

Since the spherical perturbation wave is localized in time and space, the expression for the modulating envelope of the *j*th spherical wave

$$W_{dj}(t, R) = \exp\left[-\left(\frac{(R - R_s) - R_{wj}(t)}{R_{dj}}\right)^2\right], \quad (15)$$

is the Gaussian dependence on $(R - R_s)$, where $R_{wj}(t) = V_j \times (t - t_s)$ is the propagation radius of the *j*th spherical perturbation wave at moment *t* (the mean of Gaussian curve $W_{dj}(t, R)$ at moment *t*), $R_{dj} = V_j t_d$ is the spatial half-thickness of the envelope for the *j*th spherical wave (the rms deviation of Gaussian curve $W_{dj}(t, R)$), and t_d is the duration of the total wave packet.

4. DETERMINATION OF THE IP CHARACTERISTICS

The desired IP characteristics (V, Φ_s, Λ_s, h_s) are included in the set of input parameters of the above model. An algorithm for determining these characteristics includes choosing the values of these parameters such that the model TEC variation temporal series $\Delta I_i^m(t)$ best fit the experimental TEC variation temporal series $\Delta I_i(t)$. The choice of input parameters is accomplished in several stages.

At the first stage, we determine a range of possible values of the desired parameters. On the basis of the data obtained in [3–13] for the SAW-induced IP, we assume that the possible values of IP phase velocity V range from 600 to 1200 m/s. The range of possible values of the SAW source coordinates is determined by the region centered at the earthquake epicenter and having the following parameters: a latitude of 5° and a longitude of 5°. The following two values (corresponding to the known concepts of the mechanism responsible for ionospheric perturbations following the earthquake) of the IP source altitude were considered: $h_s = 0$ (the IP source is assumed to be on the Earth's surface) and h_s = 100 km (the equivalent IP source at the time of the earthquake is assumed to be at altitudes of about 100 km) [12]. The switch-on time t_s of the IP source is assumed to be equal to time t_0 of an underground shock.

At the next stage, for values V, Φ_s, Λ_s, and h_s fixed within the range of possible values, we choose the relationship between values T, t_d, and φ such that the shape of the model ionospheric response to SAWs corresponds to that obtained from the GPS measurements. Having found this relationship, we fix the values of T, t_d, and φ.

Then, we provide for the best agreement between the temporal series $\Delta I_i^m(t)$ and $\Delta I_i(t)$ by choosing parameters Φ_s, Λ_s, V, and h_s from the range of their possible values. To estimate the correspondence, it would be appropriate to calculate the correlation function for these temporal series; however, the computation of this function for each GPS receiver–satellite LOS requires considerable computer resources and is time-consuming. To simplify this problem, we determine time $t_{\max,i}^m$ and time $t_{\max,i}$ of the maximum TEC perturbations for variations $\Delta I_i^m(t)$ and $\Delta I_i(t)$, respectively. The criterion of the minimum rms error ϵ

$$\epsilon = \sqrt{\frac{1}{P}\sum_{i=1}^{P}(t_{\max,i} - t_{\max,i}^m)^2} \quad (16)$$

is used as a goodness-of-fit test for the model and measured TEC variations. Then, we assume that the desired IP characteristics are the values of model input parameters V, Φ_s, Λ_s, and h_s such that ϵ is minimal.

For the South Sumatra earthquake, temporal series $\Delta I_i^m(t)$ best fit $\Delta I_i(t)$ or all of the GPS receiver–satellite LOSs where the ionospheric responses were recorded when the following input parameters were used in simulations: $N_w = 1$, $A = 40\%$ of N_{max}, $T = 240$ s, $t = 180$ s, $\varphi = -0.5\pi$, $V = 700$ m/s, $\Phi_s = 4.8°$ S, $\Lambda_s = 102°$ E, $h_s = 0$, and $t_s = t_0 = 16.475$ UT. Here, the value of ϵ (0.032 h) is minimal. The model TEC variations for four GPS receiver–satellite LOSs are shown in Figs. 1a–1d (the dashed line). The obtained values of V, Φ_s, Λ_s, and ϵ are summarized in Table 2.

As in the case of ionospheric responses recorded during GPS measurements, coordinates Φ_i^m and Λ_i^m of the model responses are assumed to be the coordinates of the projection of the point of intersection of the GPS receiver–satellite LOS with the plane where the *F*-region of the ionosphere has the maximum electron density on the Earth's surface at moment $t_{\max,i}^m$. The values of $t_{\max,i}^m$, Φ_i^m, and Λ_i^m for each GPS receiver–satellite LOS are presented in Table 1. In Fig. 2, the locations of the model responses are denoted by black triangles and time $t_{\max,i}^m$ is underlined.

5. MODEL TESTING

In order to test our model and graphically represent the dynamics of the IP front propagation at the time of the earthquake, we simulate the space–time distribu-

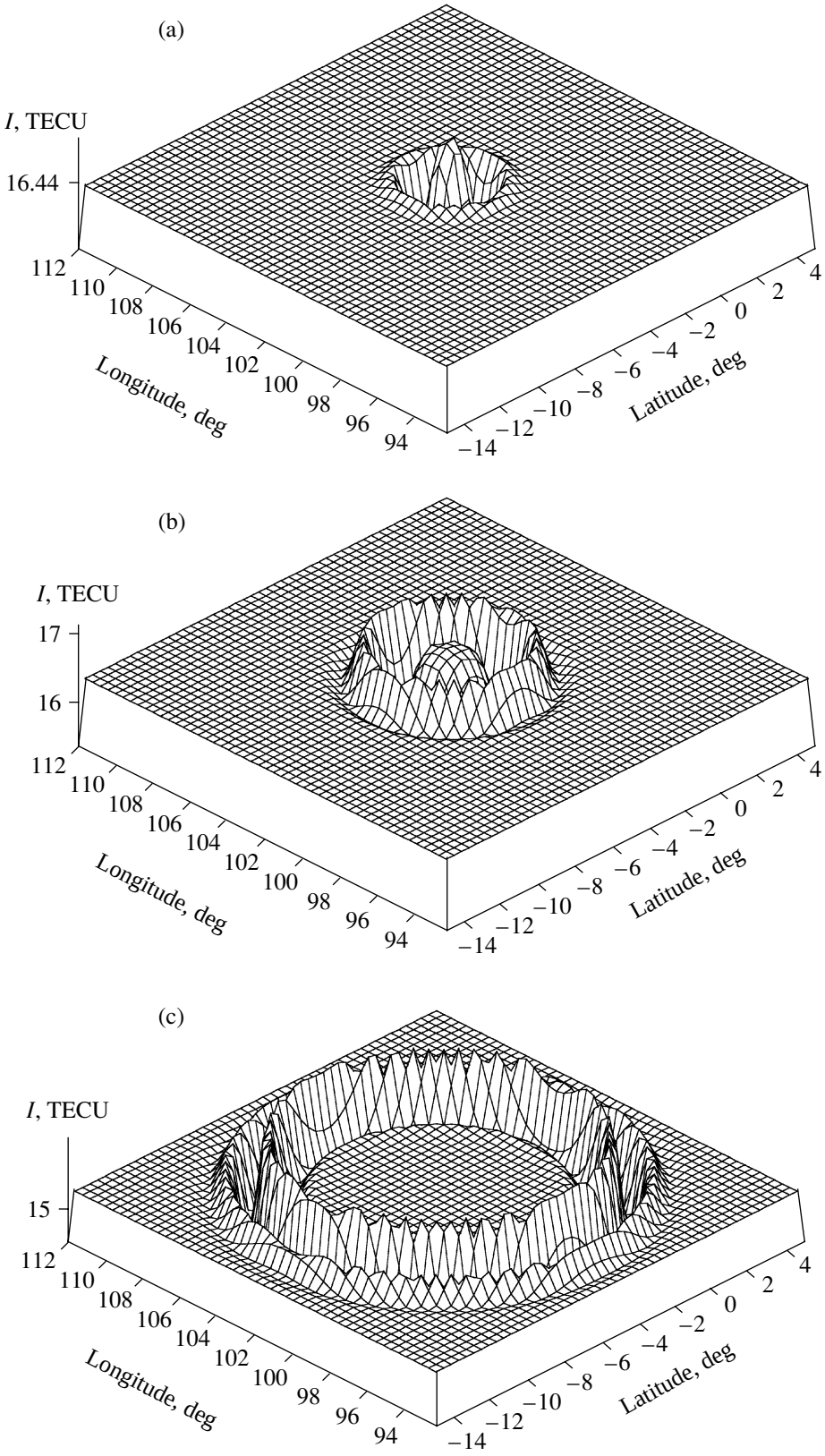

Fig. 3. The spatial distribution of the simulative values of the vertical TEC in the region of the earthquake epicenter for the observation moments (a) 16.485, (b)16.6, and (c)16.8 UT; (a): dt = 36 s, R_w = 25 km, R_l = 0, and R_u = 275 km; (b): dt = 450 s, R_w = 315 km, R_l = 165 km, and R_u = 565 km; and (c): dt = 1170 s, R_w = 820 km, R_l = 570 km, and R_u = 1070 km.

tions of the vertical TEC (at $\theta_{sat} = 90°$) in the region of the earthquake epicenter. The testing simulation was performed ignoring the daily variations of N_t with the IP parameters typical of this earthquake (see Section 4).

The model spatial TEC distribution was obtained for the following three observation moments: $t_1 = 16.485$ UT (Fig. 3a); $t_2 = 16.6$ UT (Fig. 3b), and $t_3 = 16.8$ UT (Fig. 3c). The results presented in Fig. 3 show that the TEC perturbation caused by the earthquake is a wave packet propagating from the SAW source. Now, let us analyze the dynamics of the TEC variations above the earthquake epicenter. In the simulations, we assume that the wave packet of the spherical SAW is bounded by radii $R_l = R_w - 2R_d$ and $R_u = R_w + 2R_d$ and the ionospheric region considerably contributing to the TEC formation is determined by the height range from $h_l = h_{max} - 2h_d$ to $h_u = h_{max} + 2h_d$.

For each observation moment (Fig. 3), we present the corresponding values of delay dt relative to the switch-on time of the SAW source, SAW propagation radius R_w, and lower- (R_l) and upper-boundary (R_u) radii of the SAW packet. The simulation was performed for $h_{max} = 300$ km and $h_d = 100$ km. At the moments when the spherical SAW packet is at least partly located within the ionospheric region considerably contributing to the TEC formation above the earthquake epicenter, the presence of the maximum or minimum of the TEC perturbation amplitude above this characteristic point is determined by the relationship between the following simulation parameters: T, t_d, and φ. As the overlapping region of the intervals $[R_l, R_u]$ and $[h_l, h_u]$ increases and the value of R_w approaches h_{max}, the TEC amplitude grows (see Figs. 3a, 3b). This growth is due to the electron concentration distribution over height: the lower layers with a small electron content contribute less to the TEC formation than the maximum electron density region. As the spherical SAW packet propagates further, it gradually goes out of the ionospheric region bounded by heights h_l and h_u, which results in a decrease in the TEC variation amplitude. When R_w reaches the value such that R_l exceeds h_u, the TEC returns to its unperturbed state (see Fig. 3c). A further change in the TEC distribution results in the increasing radius of the structure shown in Fig. 3c.

6. DISCUSSION OF THE RESULTS

The IP source coordinates determined using space–time processing ($\Phi_s = -4.0°$ and $\Lambda_s = 102.0°$) and simulation ($\Phi_s = -4.8°$ and $\Lambda_s = 102.1°$) and the coordinates of the earthquake epicenter ($\Phi_e = -4.72°$ and $\Lambda_e = 102.1°$) are in good agreement. The accuracy of the IP source coordinates found by these methods is 80 and 10 km, respectively.

A noticeable discrepancy between the IP phase velocities obtained using the above methods is observed. The phase velocity determined by space–time processing is $V = 1050$ m/s, and the corresponding value obtained by simulation is $V = 700$ m/s. The reason for this discrepancy between the results is in the specific features of the methods for determining the spatial–temporal perturbation characteristics.

Space–time processing allows determining the IP velocity at the altitudes of the maximum electron density region (in the *F*-region) of the ionosphere. The phase velocity $V = 1050$ m/s obtained by this method corresponds to the sound velocity $W = 950$–1000 m/s [18] at the altitude $h = 300$–400 km and agrees with the results presented in [12, 13]. In these papers, the SAW phase velocity measured by means of GPS arrays in the far-field zone of the epicenters of the August 17, 1999, and November 12, 1999, Turkey earthquakes was $V = 1173$ m/s and $V = 1157$ m/s, respectively.

In the simulations, we assume that the SAW propagation velocity is constant at all the heights (from the Earth's surface to h_u) where the ionosphere substantially contributes to the TEC formation. In the case of the earthquake under study, $h_u = 500$ km. Therefore, the IP velocity $V = 700$ m/s found from simulations is consistent with the sound velocity $W = 740$ m/s averaged over heights h in the interval 0–500 km [18].

The results obtained in this work demonstrate the efficiency of the methods proposed for determining the spatial–temporal characteristics of the IP recorded in the near-field region of the source and once again confirm the sonic nature of the earthquake-generated IPs.

ACKNOWLEDGMENTS

The authors are grateful to A.V. Plotnikov for help in the primary data processing. This work was supported by the Russian Foundation for Basic Research (project nos. 99-05-64753 and 00-05-72026) and the Leading Scientific Schools of the Russian Federation (grant 00-15-98509).

REFERENCES

1. Nagorskii, P.M., *Geomagn. Aeron.*, 1998, vol. 38, p. 100.
2. Afraimovich, E.L., Varshavskii, I.I., Vugmeister, B.O., *et al.*, *Geomagn. Aeron.*, 1984, vol. 24, p. 322.
3. Jacobson, A.R. and Carlos, R.C., *J. Atmos. Solar–Terr. Phys.*, 1994, vol. 56, p. 525.
4. Mendillo, M., *Adv. Space Res.*, 1981, vol. 1, p. 275.
5. Mendillo, M., *Adv. Space Res.*, 1982, vol. 2, p. 150.
6. Li, Y.Q., Jacobson, A.R., Carlos, R.C., *et al.*, *Geophys. Res. Lett.*, 1994, vol. 21, p. 2737.
7. Calais, E. and Minster, J.B., *Geophys. Res. Lett.*, 1995, vol. 22, p. 1045.
8. Calais, E. and Minster, J.B., *Geophys. Res. Lett.*, 1996, vol. 23, p. 1897.
9. Afraimovich, E.L., Kosogorov, E.A., Palamartchouk, K.S., *et al.*, *Earth Planets Space*, 2000, vol. 52, no. 11, p. 1061.

10. Fitzgerald, T.J., *J. Atmos. Solar–Terr. Phys.*, 1997, vol. 59, p. 829.
11. Calais, E., Minster, B.J., Hofton, M.A., and Hedlin, M.A.H., *Geophys. J. Int.*, 1998, vol. 132, p. 191.
12. Afraimovich, E.L., Perevalova, N.P., Plotnikov, A.V., and Uralov, A.M., *Ann. Geophys.* (France), 2001, vol. 19, no. 4, p. 395.
13. Afraimovich, E.L., Kosogorov, E.A., Plotnikov, A.V., and Uralov, A.M., *Fiz. Zemli*, 2001, no. 6, p. 1.
14. Afraimovich, E.L., Kiryushkin, V.V., and Chernukhov, V.V., *Radiotekh. Elektron.* (Moscow), 2001, vol. 46, no. 11, p. 1299.
15. Row, R.V., *J. Geophys. Res.*, 1967, vol. 72, no. 5, p. 1599.
16. Afraimovich, E.L., Palamartchouk, K.S., and Perevalova, N.P., *J. Atmos. Solar–Terr. Phys.*, 1998, vol. 60, no. 12, p. 1205.
17. Bakulin, P.I., Kononovich, E.V., and Moroz, V.I., *Kurs obshchei astronomii* (General Astronomy Course), Moscow: Nauka, 1966.
18. Gossard, E. and Hooke, W., *Waves in the Atmosphere*, Amsterdam: Elsevier, 1975. Translated under the title *Volny v atmosfere*, Moscow: Mir, 1978.